

TensoSDF: Roughness-aware Tensorial Representation for Robust Geometry and Material Reconstruction

JIA LI, School of Software, Shandong University, China

LU WANG[†], School of Software, Shandong University, China

LEI ZHANG, The Hong Kong Polytechnic University, China

BEIBEI WANG[†], School of Intelligence Science and Technology, Nanjing University, China

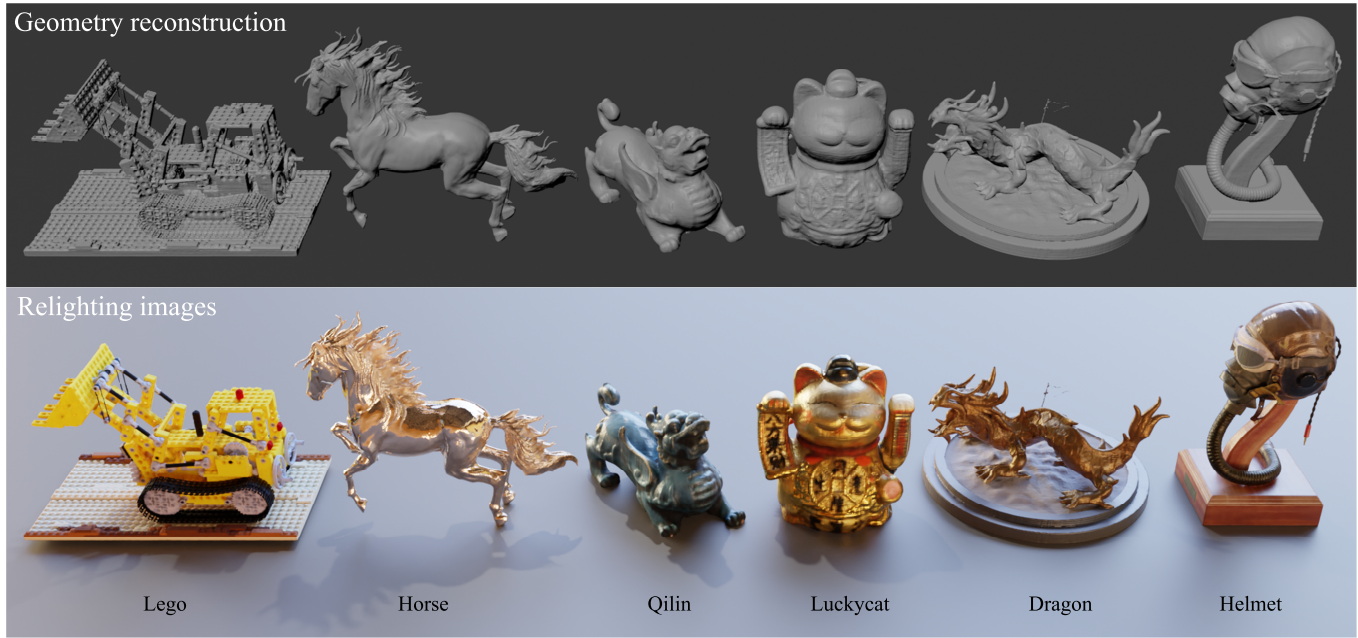


Fig. 1. We present a roughness-aware tensorial representation for robust geometry and material reconstruction from multi-view images. In this scene, we showcase six objects with different materials, including diffuse LEGO from TensoIR [Jin et al. 2023], specular HORSE from NeRO [Liu et al. 2023], and several glossy objects from NeLF++ [Zhang et al. 2023] and our datasets, where QILIN and LUCKYCAT are real data. Our method demonstrates robust reconstruction of any reflective objects, detailed geometry results and faithful material estimation, leading to photo-realistic relighting.

Reconstructing objects with realistic materials from multi-view images is problematic, since it is highly ill-posed. Although the neural reconstruction approaches have exhibited impressive reconstruction ability, they are designed for objects with specific materials (e.g., diffuse or specular materials). To this end, we propose a novel framework for robust geometry and material

[†]Corresponding authors.

Authors' addresses: Jia Li, School of Software, Shandong University, China, riga27527@gmail.com; Lu Wang[†], School of Software, Shandong University, China, luwang_hcivr@sdu.edu.cn; Lei Zhang, The Hong Kong Polytechnic University, China, cslzhang@comp.polyu.edu.hk; Beibei Wang[†], School of Intelligence Science and Technology, Nanjing University, China, beibei.wang@nju.edu.cn.

Permission to make digital or hard copies of all or part of this work for personal or classroom use is granted without fee provided that copies are not made or distributed for profit or commercial advantage and that copies bear this notice and the full citation on the first page. Copyrights for components of this work owned by others than the author(s) must be honored. Abstracting with credit is permitted. To copy otherwise, or republish, to post on servers or to redistribute to lists, requires prior specific permission and/or a fee. Request permissions from permissions@acm.org.

© 2024 Copyright held by the owner/author(s). Publication rights licensed to ACM. 0730-0301/2024/7-ART150 \$15.00
https://doi.org/10.1145/3658211

reconstruction, where the geometry is expressed with the implicit signed distance field (SDF) encoded by a tensorial representation, namely *TensoSDF*. At the core of our method is the roughness-aware incorporation of the radiance and reflectance fields, which enables a robust reconstruction of objects with arbitrary reflective materials. Furthermore, the tensorial representation enhances geometry details in the reconstructed surface and reduces the training time. Finally, we estimate the materials using an explicit mesh for efficient intersection computation and an implicit SDF for accurate representation. Consequently, our method can achieve more robust geometry reconstruction, outperform the previous works in terms of relighting quality, and reduce 50% training times and 70% inference time. Codes and datasets are available at <https://github.com/Riga2/TensoSDF>.

CCS Concepts: • **Computing methodologies** → **Rendering**.

Additional Key Words and Phrases: neural rendering, multiview reconstruction

ACM Reference Format:

Jia Li, Lu Wang[†], Lei Zhang, and Beibei Wang[‡]. 2024. TensoSDF: Roughness-aware Tensorial Representation for Robust Geometry and Material Reconstruction. *ACM Trans. Graph.* 43, 4, Article 150 (July 2024), 13 pages. <https://doi.org/10.1145/3658211>

1 INTRODUCTION

Reconstructing objects with realistic materials from multi-view images is a fundamental and challenging task in computer graphics and computer vision. However, due to their highly ill-posed nature, the existing approaches have difficulty decoupling the geometries and materials. Starting from Neural Radiance Field (NeRF) [Mildenhall et al. 2021], the neural rendering-based approaches have brought a significant opportunity for this task and exhibit impressive reconstruction capability.

These neural reconstruction methods reconstruct the geometries and materials by representing geometries with an implicit function (e.g., density or SDF field) encoded by multi-layer perception (MLP) and modeling the color distribution with a radiance field or a reflectance field. Then, they learn these representations via differentiable rendering, supervised by the multi-view images. These two representations are the key to reconstruction. For the geometry representation, the density-field based methods [Boss et al. 2021a; Jin et al. 2023; Srinivasan et al. 2021; Verbin et al. 2022; Zhang et al. 2021b] have achieved remarkable performance on the novel view synthesis (NVS) and material estimation, while the quality of the reconstructed surface is inferior. The underlying reason is the lack of surface constraints, leading to noisy surfaces and inaccurate surface normals, especially for specular surfaces. In contrast, the SDF-based approaches show superior quality on the reconstructed surfaces.

Among the previous SDF-based methods, several approaches [Wang et al. 2021, 2023; Yariv et al. 2021; Zhang et al. 2021a, 2022a] rely on radiance-field for surface reconstruction. These methods are effective on non-specular surfaces but fail on objects with strong reflections. The other line of work (e.g., NeRO [Liu et al. 2023] and NeILF++ [Zhang et al. 2023]) model the reflection of surface explicitly with the rendering equation [Kajiya 1986], leading to a much higher reconstruction quality for highly-specular objects. Despite the benefits of reconstructing specular objects, leveraging the reflectance field is not stable enough to optimize and easily falls into local optimum, leading to erroneous geometry. Therefore, no existing approaches can achieve compelling results on objects with arbitrary reflective materials (no translucent).

In this paper, we propose a novel framework for robust geometry and material reconstruction on top of NeRO [Liu et al. 2023], including a geometry reconstruction step, followed by a material estimation step. At the core of our framework is a deep incorporation of the radiance and reflectance fields for arbitrary surface reconstruction. To this end, we propose a roughness-aware combination of these two fields. Furthermore, we introduce a tensorial representation for SDF (i.e., *TensoSDF*), enabling a more detailed reconstructed surface and reducing the training time to about 50%. Finally, with the reconstructed geometry, we use an explicit-implicit fusion strategy to estimate the material, which uses the explicit mesh as a proxy for efficient ray-intersection computation and the implicit SDF field for more accurate geometric representation, further

improving estimated material quality. Consequently, our method can achieve more robust geometry reconstruction and outperform the previous works in terms of relighting quality. To summarize, our main contributions include:

- we propose roughness-aware incorporation of the radiance and reflectance field for robust geometry reconstruction on any reflective objects.
- we introduce a novel representation – *TensoSDF*, that combines the tensorial representation with SDF, enabling more detailed geometry reconstruction and reducing training time.
- we design an explicit-implicit fusion strategy for material estimation, combining the explicit mesh and implicit SDF field, further improving the quality of reconstructed materials.

2 RELATED WORK

Neural geometry reconstruction. Existing geometry reconstruction methods from multi-view images include the traditional ones [Barron and Poole 2016; Bleyer et al. 2011; Campbell et al. 2008; Furukawa and Ponce 2007; Gallup et al. 2007; Hosni et al. 2012; Richardt et al. 2010; Schonberger and Frahm 2016; Strecha et al. 2006] and recent neural approaches [Li et al. 2023; Niemeyer et al. 2020; Oechsle et al. 2021; Wang et al. 2021; Wu et al. 2022; Yariv et al. 2023, 2020]. With the advances in neural rendering [Mildenhall et al. 2021], the neural approaches have shown impressive reconstruction results. In this paper, we focus on neural geometry reconstruction methods. These methods usually use a neural implicit function to express scene geometry, such as the density field [Boss et al. 2021a; Jin et al. 2023; Mildenhall et al. 2021; Verbin et al. 2022; Zhang et al. 2021b], signed distance field [Li et al. 2023; Wang et al. 2021, 2023; Yariv et al. 2023, 2020] or occupancy field [Niemeyer et al. 2020; Oechsle et al. 2021], and use a neural color function for differentiable rendering. We categorize these methods into two groups according to their color function: *radiance field* that implicitly encodes the color with the view direction and surface geometry, and *reflectance field* that explicitly incorporates the formulation of the rendering equation [Kajiya 1986].

Among the radiance-field methods, DVR [Niemeyer et al. 2020] and IDR [Yariv et al. 2020] first introduce surface rendering with occupancy function or SDF for 3D geometry reconstruction, respectively. However, these methods need pixel-accurate object masks for surface estimation. Later, NeuS [Wang et al. 2021], VolSDF [Yariv et al. 2021] and UNISURF [Oechsle et al. 2021] solve this problem by incorporating the volume-rendering framework from NeRF [Mildenhall et al. 2021], and can obtain decent reconstructed results. With the advent of the explicit representation [Chen et al. 2022; Müller et al. 2022; Sun et al. 2022], Voxurf [Wu et al. 2022], NeuS2 [Wang et al. 2023], Neuralangelo [Li et al. 2023] and BakedSDF [Yariv et al. 2023] are proposed to improve the geometry quality further and reduce the training time. All these methods have shown remarkable results in reconstructing non-specular objects but fail on objects with strong reflections.

The reflectance-field methods usually require many assumptions to decompose the color into the light and materials. Ref-NeRF [Verbin et al. 2022] decomposes the color into diffuse and specular terms, and uses integrated direction encoding to improve the NVS quality

on reflective objects. TensoIR [Jin et al. 2023] adopts the efficient TensoRF [Chen et al. 2022] framework to explicitly model indirect lights, achieving good geometry reconstruction on diffuse surfaces. These two methods are all based on density field, which has inferior quality on the geometry reconstruction of specular objects. Recently, NeRO [Liu et al. 2023] designed a novel light representation based on split-sum approximation [Karis and Games 2013], leading to high-quality geometric results on highly-specular objects. However, NeRO easily falls into the local optimum and causes erroneous geometry. NeILF++ [Zhang et al. 2023] proposes to marry an incident light field and an outgoing radiance field via physical-based rendering, enables handling specular surfaces and inter-reflections, but often causes over-smooth results and costs a long time to train.

Neither of the above two types of methods can achieve compelling results on objects with arbitrary reflective materials. In contrast, our method is robust and can handle any reflective objects by learning the radiance and reflectance fields together.

Neural material estimation. Existing material estimation methods from multi-view images are mainly based on the inverse rendering framework. Most of them [Boss et al. 2021a,b; Zhang et al. 2021a] only consider the direct light for rendering to save computation, while lowering the quality. NeRV [Srinivasan et al. 2021] considers the visibility and indirect light but requires multiple known lighting conditions. NeRFactor [Zhang et al. 2021b] can handle unknown illumination but without considering indirect light. To model the indirect light, MII [Zhang et al. 2022a] uses Spherical Gaussian to represent the indirect illumination, NDRMC [Hasselgren et al. 2022] explicitly samples secondary ray with a denoiser, NeILF [Yao et al. 2022] and NeILF++ [Zhang et al. 2023] represent scene lightings with a neural incident light field, and TensoIR [Jin et al. 2023] resorts to efficient TensoRF [Chen et al. 2022] framework. All these methods improve the quality of estimated materials but produce inferior results on highly reflective objects. NeRO [Liu et al. 2023] estimates the material using Monte Carlo integration with importance sampling on the fixed mesh, which can produce decent results on reflective objects. However, explicit mesh suffers from geometry degradation, causing apparent biases in the estimated materials. In comparison, we unify the explicit mesh and implicit SDF field for material estimation, further improving the quality of reconstructed materials.

3 BACKGROUND

In this section, we briefly review NeuS and NeRO [Liu et al. 2023], since we are related to their work. They both represent the geometry with a neural SDF field, and the underlying surface is the zero-level set of the SDF. Then, they use different ways to reconstruct their surface.

NeuS. The geometry is reconstructed by performing the volume rendering [Mildenhall et al. 2021] with the radiance field. Specifically, given the camera origin o and view direction d of each pixel, NeuS samples n points along the ray $\{p_i = o + t_i d \mid t_i > 0, t_{j-1} < t_j\}$, and then aggregates the contribution of these points to form the pixel

color C :

$$C = \sum_{i=0}^n w_i c_i, \quad (1)$$

where w_i is the weight of the i -th point, derived from the SDF value, and c_i is the radiance at this point from the radiance field encoded with a color network. Then, the geometry and the radiance networks can be learned by minimizing the loss between the rendered color C and the ground truth color C_{gt} :

$$\ell = \|C - C_{\text{gt}}\|_2^2. \quad (2)$$

NeRO. Unlike NeuS, NeRO [Liu et al. 2023] explicitly incorporates the rendering equation [Kajiya 1986] in neural reconstruction using a reflectance field to reconstruct specular objects better. In particular, NeRO reconstructs the geometry by employing a split-sum approximation [Karis and Games 2013] to evaluate the rendering equation. Then, they extract the mesh and perform the Monte Carlo integration to estimate the materials on the extracted meshes.

Despite NeRO’s impressive capability on high specular objects, their model easily falls into the local optimum, resulting in erroneous geometry, due to the extensive assumption from the shading model and light transport. Moreover, the pure MLP-based representation leads to over-smooth geometry and a long training time.

4 METHOD

In this section, we present our approach, following the similar pipeline (a geometry reconstruction step and a material estimation step) as NeRO, but with several key differences, as shown in Fig. 2. We introduce a tensorial representation for SDF (Sec. 4.1) and then propose to incorporate the radiance and reflectance fields for surface reconstruction (Sec. 4.2). After reconstructing the geometry, we unify the explicit mesh and the implicit SDF field for material estimation (Sec. 4.3).

4.1 TensoSDF representation

To represent the geometry of the object, our goal is to find an high-capacity and efficient representation. Hence, we introduce a new representation for the SDF – TensoSDF, combining the tensorial representation with SDF to replace the original MLP encoded ones. A well-known issue of the tensorial representation is the noisy reconstruction surface, due to the lack of global correlation. To alleviate this problem, we further introduce two smoothness priors to reduce the noise.

Tensorial representation. We use the Vector-Matrix factorization proposed by TensoRF [Chen et al. 2022] as our tensorial encoder. Since SDF is a continuous function, directly using pure explicit representation to model the SDF field leads to unstable training. To address this issue, we use a small MLP as a decoder after tensorial encoding. Moreover, different from TensoRF, which uses two separate tensor grids to encode the geometry and appearance, we leverage one shared tensorial encoder and MLP decoder, which can enhance the correlation between the geometry and appearance. Our tensorial representation is formulated as follows:

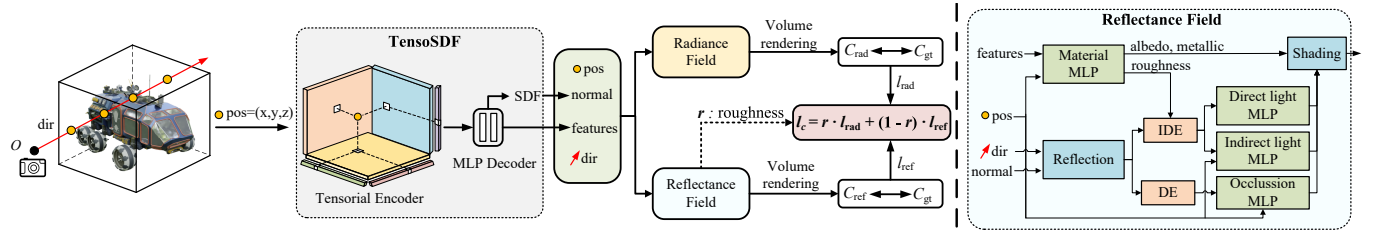


Fig. 2. The network architecture in our geometry reconstruction step. The core of our network is the TensorSDF (on the left), consisting of a tensorial encoder and an MLP decoder, which maps the position of sampled points to SDF values and appearance features. This TensorSDF representation is learned by incorporating the radiance and reflectance fields with the *roughness* as a balancing weight. Specifically, the joint loss l_c is designed to combine two color losses l_{rad} and l_{ref} , which are computed by rendering the radiance and reflectance fields, respectively. The structure of the reflectance field is shown on the right.

$$V_p = v_k^X \circ M_k^{YZ} \oplus v_k^Y \circ M_k^{XZ} \oplus v_k^Z \circ M_k^{XY}, \quad (3)$$

$$\{s, v_f\} = \Theta(V_p, p), \quad (4)$$

where v_k^m and $M_k^{\bar{m}}$ represent the k -th vector and matrix factors of their corresponding spatial axes m , and \bar{m} denotes the two axes orthogonal to m (e.g., $\bar{X} = YZ$). \circ and \oplus represent the element-wise multiplication and concatenation operations. V_p is the latent vector from the tensorial encoder and then is decoded with the position p by a tiny MLP Θ to get the SDF value s and the appearance feature v_f .

Smoothness priors. With the TensorSDF, we further introduce two strategies during training and inference to alleviate the noise issue. First, during training, we introduce a Gaussian smooth loss on the tensor grid, which is expressed as follows:

$$\ell_g = \sum_{k=1}^K \|G(M_k | k_g, \sigma_g) - M_k\|_2^2 + \|G(v_k | k_g, \sigma_g) - v_k\|_2^2, \quad (5)$$

where G is denoted as a 2D Gaussian convolution with kernel size k_g and standard deviation σ_g . In this way, the local consistency of the tensor grid can be enhanced.

After training the SDF field, we construct a two-layer mipmap of the tensor grid by performing the bilinear interpolation. When extracting the mesh by Marching Cube [Lorenson and Cline 1998], we compute the final SDF \hat{s} by blending the SDF value s by Eqn. (3) from the base tensor grid and the other one s' from the top layer with weight α :

$$\hat{s} = (1 - \alpha) \cdot s + \alpha \cdot s', \quad (6)$$

$$s' = \Theta(V'_p, p), \quad (7)$$

where V'_p is the latent vector at the top layer. As a result, the extracted mesh is much smoother while keeping the details.

4.2 Incorporating the radiance and reflectance fields

The explicit incorporation of the rendering equation in NeRO [Liu et al. 2023] enables a high-quality reconstruction of specular objects since it can express the high-frequency angular effects better than using the implicit color function directly (i.e., radiance field). However, we notice that this reflectance field is unstable and falls into the local optimum, resulting in erroneous geometry. The underlying

reason is that for objects with smooth angular effects, the implicit color function better fits the multi-view observations due to the extensive assumptions of the shading model and light transport for the explicit rendering. Hence, we propose incorporating both the reflectance and radiance fields. The main question is how to fuse these two fields. One straightforward way is weighting them with a fixed weight; however, it shows inferior reconstructed quality. To this end, we propose a simple yet effective way, leveraging the roughness at each point as a balance factor.

Radiance field & reflectance field. We follow the NeuS [Wang et al. 2021] to model our radiance field:

$$c_{rad} = \Theta_{rad}(p, n, v_f, d). \quad (8)$$

Here, Θ_{rad} is the radiance MLP, p is a sample position, n is the normal at p derived from the SDF value, v_f is the appearance features output from the TensorSDF (Eqn. (3)) and d is the view direction.

Then, we utilize the reflectance field from NeRO [Liu et al. 2023], as shown on the right in Fig. 2, which can be formulated as:

$$\{a, m, r\} = \Theta_{mat}(p, v_f), \quad (9)$$

$$L_d = \Theta_{direct}(n), \quad (10)$$

$$L_{ind} = \Theta_{indirect}(p, w_r, r), \quad (11)$$

$$u = \Theta_{occ}(p, w_r), \quad (12)$$

$$c_{ref} = \rho_{diff} \cdot L_d + \rho_{spec} \cdot ((1 - u) \cdot L_d + u \cdot L_{ind}), \quad (13)$$

where Θ_{mat} is the material MLP which outputs albedo a , metallic m and roughness r . Θ_{direct} and $\Theta_{indirect}$ are the direct-light MLP and indirect-light MLP, respectively. u is the occlusion probability from the occlusion MLP Θ_{occ} . w_r is the reflected view direction around the normal n . ρ_{diff} and ρ_{spec} are the diffuse and specular terms from the microfacet BRDF [Cook and Torrance 1982] respectively.

Roughness-aware learning. With both the radiance color c_{rad} and reflectance color c_{ref} at each sampled point, we compute two aggregated pixel colors by Eqn. (1): C_{rad} and C_{ref} . Then, we compute their own loss w.r.t. the multi-view images by Eqn. (2): l_{rad} and l_{ref} , respectively. To balance the learning of the radiance field and reflectance field, we introduce roughness from Eqn. (9) as the balancing factor into the final loss, formulated as:

$$l_c = r \cdot l_{rad} + (1 - r) \cdot l_{ref}. \quad (14)$$

The gradient of roughness r is detached here for stable optimization. In this way, our model can adaptively adjust the learning weights of two fields according to the surface roughness, enabling robust reconstruction of any reflective objects.

4.3 Unifying mesh and SDF for material estimation

We now have reconstructed the faithful geometry but with a rough material. A simple way to achieve more accurate material is following NeRO directly by evaluating the Monte Carlo integration with importance sampling using the extracted mesh due to its ray-intersection efficiency. However, using the extracted mesh for material estimation leads to geometry degradation. On the other hand, using the implicit SDF field with volume rendering is too time-consuming, even under the tensorial representation, due to the exponential-increasing computation and memory cost for the indirect lighting.

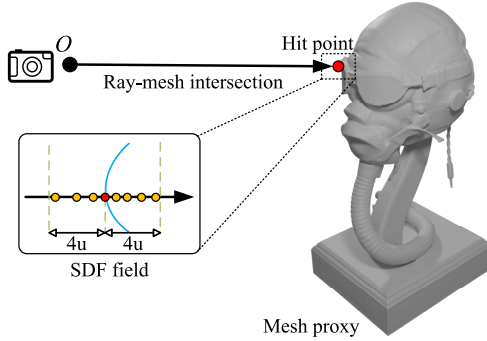


Fig. 3. Illustration of our mesh-SDF fusion strategy. First, we perform ray-mesh intersection to get a rough hit point. Then, we sample m points within a fixed distance inside and outside the surface.

To avoid this problem, we use explicit mesh as a proxy to get a rough hit point by fast ray-mesh intersection and then perform volume rendering on the neighbor of the hit surface, as shown in Fig. 3. Here, we sample m points within the distance of $4u$ inside and outside the surface, where u is the unit size of the tensor grid. Then, we perform volume rendering to get the accurate hit point \hat{p} and its surface normal \hat{n} :

$$\hat{t} = \sum_{i=0}^m w_i t_i, \quad (15)$$

$$\hat{n} = \sum_{i=0}^m w_i n_i, \quad (16)$$

$$\hat{p} = o + \hat{t}d. \quad (17)$$

Here t_i and n_i are the depth and normal of i -th sampled point.

Thanks to the mesh and implicit SDF combination, our method can achieve more accurate material estimation while maintaining time efficiency.

5 IMPLEMENTATION DETAILS

In this section, we present our datasets, network structures, and training details.

Datasets. To validate our method, we propose a new synthetic dataset consisting of six scenes with various typical material types (diffuse, glossy, and specular). We render these scenes to generate their ground-truth images, normal maps, and relighting images under five environment lights using the Cycles renderer in Blender. Moreover, we also evaluate our method on datasets from TensoIR [Jin et al. 2023] and NeRO [Liu et al. 2023], which mainly focus on diffuse or specular scenarios, respectively. For the real datasets, we use the NeILF-HDR dataset from NeILF++ [Zhang et al. 2023] and Stanford-ORB dataset [Kuang et al. 2024]. We adopt the ACES tone mapping [Gatta et al. 2002] to obtain the low-dynamic range (LDR) images from the NeILF-HDR dataset, since the high-dynamic range (HDR) images are unnecessary in our experiments. The Stanford-ORB dataset includes ground-truth captured meshes and relighting images, and we choose its LDR images for our experiments.

Network structures. The TensoSDF has a resolution of 512×512 with the feature channels set as 36. The decoder is a two-layer MLP with a width of 128. The MLP networks in the radiance and reflectance fields (Eqn. (8) and Eqn. (9)) all have three layers with widths of 128.

Training. We define different losses for the geometry reconstruction and the material estimation stages. The loss function at the geometry reconstruction stage includes a color loss ℓ_c (Eqn. (14)), a Gaussian smooth loss ℓ_g (Eqn. (5)), and an Eikonal loss ℓ_e for valid SDF learning [Gropp et al. 2020]. We also use a total variation (TV) loss ℓ_t from TensoRF [Chen et al. 2022], occlusion loss ℓ_o and stabilization loss ℓ_s from NeRO [Liu et al. 2023] for the reflectance field optimization. Furthermore, depending on whether the object mask is available, we use a mask loss for better convergence or a Hessian loss [Zhang et al. 2022b] ℓ_h . The final loss is:

$$\ell = \ell_c + \lambda_e \ell_e + \lambda_g \ell_g + \lambda_h \ell_h + \lambda_t \ell_t + \ell_o + \ell_s, \quad (18)$$

where λ is the corresponding weight of each loss (we set $\lambda_e = \lambda_t = 0.1$, $\lambda_g = 1e^{-5}$ and $\lambda_h = 0.5$ or $5e^{-4}$ for mask loss or Hessian loss in practice).

The loss function at the material estimation stage includes a color loss ℓ_c and a material regularization loss ℓ_m from NeRO [Liu et al. 2023]:

$$\ell = \ell_c + \lambda_m \ell_m, \quad (19)$$

where λ_m is the loss weight of the regularization (0.1 in practice).

During the training of the geometry reconstruction stage, we use a coarse-to-fine training strategy by setting the initial grid resolution as 128×128 and increasing to the final resolution, i.e., 512×512 . At the first 20k steps, we only learn the reflectance field to get a rough shape and an initial roughness. Then, we compute two pixel colors from the radiance and reflectance fields. We use these two colors to compute two separate losses and combine the two losses with the roughness-aware strategy by Eqn. (2). During inference, we use the reflectance field or the recovered materials to compute the final color.

We use Adam optimizer [Kingma and Ba 2014] in PyTorch [Paszke et al. 2019] with initial learning rates of 0.01 for the tensor grids and 0.001 for all the MLP networks, and use cosine learning rate scheduler with the target decay ratio 0.05. The training epochs for

the geometry stage are 180k, and for the material stage are 100k, which take an average of 4 hours and 1.5 hours on a single RTX 4090 GPU, respectively.

6 RESULTS

In this section, we first evaluate our geometry reconstruction (Sec. 6.1) and material estimation (Sec. 6.2) on the synthetic datasets. Then, we present reconstruction results on the real datasets (Sec. 6.3). We perform ablation studies to verify the effectiveness of our design (Sec. 6.4). Finally, we give the discussion of our limitations (Sec. 6.5). More results can be found in our supplementary materials and video.

6.1 Reconstructed geometry evaluation

To evaluate the geometry reconstruction quality, we adopt the mean angular error (MAE) between the reconstructed normal and the ground-truth normal as the metric and use the Chamfer distance (CD) metric on the NeRO [Liu et al. 2023] dataset. We compare our method with NeuS [Wang et al. 2021], TensoIR [Jin et al. 2023], NeRO [Liu et al. 2023] and NeILF++ [Zhang et al. 2023]. For all these methods, we use their official implementations.

In Fig. 4, we compare our method with the other four methods on our synthetic dataset. By comparison, our method can not only reconstruct the surfaces with strong reflection in all three scenes but also recover the detailed geometries (the grid in the COMPRESSOR scene and the tube in the HELMET scene). TensoIR [Jin et al. 2023] has difficulties in handling reflective surfaces, since it represents the geometry with the density field. NeRO [Liu et al. 2023] shows impressive reconstruction on simple specular objects but easily falls into local optimum for complex scenes, leading to incorrect geometries. NeuS [Wang et al. 2021] can reconstruct most non-specular surfaces except the ones with strong reflections. NeILF++ [Zhang et al. 2023] can reconstruct geometries reasonably on various materials but loses geometry details and needs a long training time (more than 12 hours for each scene). We also report the quality metrics on our synthetic dataset and the average training time in Tab. 1. Our method outperforms the other four methods on the average MAE metrics across six scenes, but has slightly higher errors than NeuS on the DRAGON and MOTOR scenes, mainly due to the noise problem. Thanks to the tensorial representation, our method achieves shorter training times than the other three methods and equals TensoIR [Jin et al. 2023].

We also conduct the comparison on the datasets from NeRO [Liu et al. 2023] and TensoIR [Jin et al. 2023], as shown in Fig. 5 and Fig. 6. Our method can handle both diffuse and specular scenes, demonstrating its robustness. Meanwhile, our method exhibits the most detailed geometry details, thanks to the TensoSDF representation.

6.2 Estimated material evaluation

Since different methods use different shading models, comparing the reconstructed materials directly is difficult. Following NeRO [Liu et al. 2023], we relight the estimated materials and compare their results with the ground truth as one effective way for validation. Specifically, we first extract the recovered meshes and materials, and re-illuminate the scene with five new environment lights in, each

Table 1. Geometry reconstruction quality in terms of normal MAE \downarrow on our synthetic dataset. **Bold** means the best performance and underline means the second best.

	NeuS	TensoIR	NeRO	NeILF++	Ours
Rover	<u>3.25</u>	3.40	5.31	3.52	3.21
Dragon	2.33	<u>2.50</u>	3.99	3.26	2.59
Motor	3.59	3.78	4.78	4.54	<u>3.70</u>
Helmet	3.45	3.45	8.27	<u>3.14</u>	2.74
Robot	2.65	2.73	5.57	<u>2.59</u>	2.04
Compressor	<u>5.09</u>	5.37	9.18	6.06	3.48
Avg. MAE	<u>3.39</u>	3.54	6.18	3.85	2.96
Avg. training time	<u>6 hrs</u>	4 hrs	8 hrs	12 hrs	4 hrs

Table 2. Relighting quality in terms of PSNR and SSIM on our synthetic dataset. **Bold** means the best performance and underline means the second best.

	TensoIR		NeRO		NeILF++		Ours	
	PSNR / SSIM	PSNR / SSIM	PSNR / SSIM	PSNR / SSIM	PSNR / SSIM	PSNR / SSIM	PSNR / SSIM	
Rover	24.000 / <u>0.918</u>	<u>24.015</u> / 0.914	23.774 / 0.911	26.754 / 0.935				
Dragon	25.104 / 0.895	<u>25.644</u> / <u>0.919</u>	24.099 / 0.901	27.899 / 0.936				
Motor	19.219 / 0.906	<u>22.158</u> / <u>0.917</u>	20.142 / 0.894	22.754 / 0.930				
Helmet	<u>25.140</u> / 0.901	22.587 / 0.881	24.001 / <u>0.906</u>	28.126 / 0.934				
Robot	<u>26.031</u> / <u>0.928</u>	23.194 / 0.913	22.696 / 0.915	26.242 / 0.940				
Compressor	20.753 / 0.868	<u>21.624</u> / <u>0.878</u>	19.740 / 0.844	24.049 / 0.916				
Avg.	<u>23.375</u> / 0.903	23.204 / <u>0.904</u>	22.41 / 0.895	25.971 / 0.932				

rendering 20 evenly distributed relighted images. We use peak signal-to-noise ratio (PSNR), structural similarity index (SSIM) [Wang et al. 2004], and learned perceptual image patch similarity (LPIPS) [Zhang et al. 2018] metrics to measure the quality of results. We compare our method against three others: TensoIR [Jin et al. 2023], NeRO [Liu et al. 2023] and NeILF++ [Zhang et al. 2023] on our synthetic dataset. We scale the relighted images with a global scalar for all the methods, as done in TensoIR [Jin et al. 2023].

The quantitative measurements are shown in Tab. 2 for PSNR and SSIM, and in our supplementary for LPIPS. We also provide the visual results in Fig. 7. By comparison, our method achieves more plausible relighting results than other methods. NeRO [Liu et al. 2023] mainly suffers from inaccurate reconstructed geometry, resulting in inferior relighting quality. On the other hand, NeILF++ [Zhang et al. 2023] and TensoIR [Jin et al. 2023] produce less-specularity materials and struggle to keep the high-frequency effects, due to their Spherical Gaussian approximation on the BRDF or environment light.

We visualize the estimated materials (albedo, roughness and metallic) on HELMET and ROBOT scenes, as shown in Fig. 8. We scale the albedo results by a global scalar, as done in TensoIR [Jin et al. 2023]. By comparison, our method can achieve the closest estimated albedo maps, and reasonable metallic and roughness maps, leading to credible relighting results.

6.3 Results on real data

We first evaluate our method on the real dataset from NeILF++ [Zhang et al. 2023], as shown in Fig. 9. We compare our method with

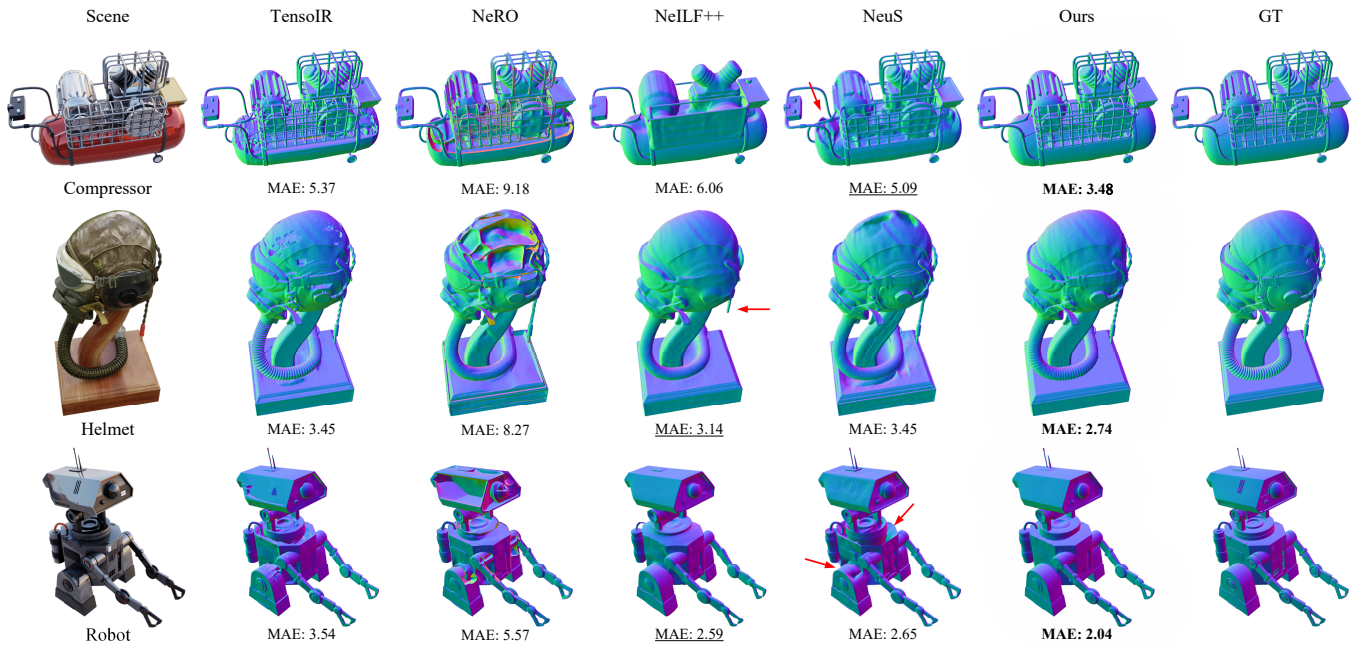


Fig. 4. Comparison of geometry reconstruction among our method, TensoIR [Jin et al. 2023], NeRO [Liu et al. 2023], NeILF++ [Zhang et al. 2023] and NeuS [Wang et al. 2021] on our synthetic dataset.

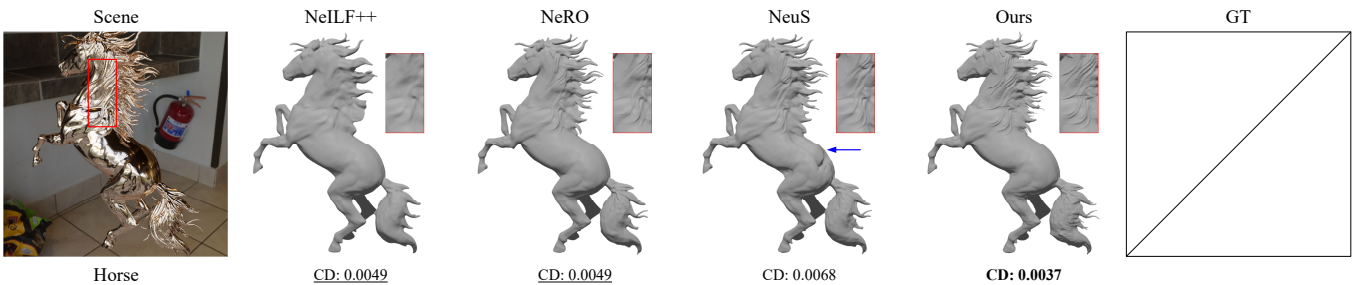


Fig. 5. Comparison of geometry reconstruction among our method, NeILF++ [Zhang et al. 2023], NeRO [Liu et al. 2023] and NeuS [Wang et al. 2021] on the scene from NeRO [Liu et al. 2023]. There is no available ground-truth mesh in NeRO dataset, and the CD_{\downarrow} loss is computed on the point cloud following NeRO [Liu et al. 2023].

NeRO [Liu et al. 2023] and NeILF++ [Zhang et al. 2023] on geometry reconstruction. Note that the input images of our method and NeRO [Liu et al. 2023] are LDR images, while NeILF++ [Zhang et al. 2023] uses the HDR images following the official implementation. By comparison, our method is able to handle surfaces with strong highlights, while NeILF++ [Zhang et al. 2023] fails (pointed by the red arrow in QILIN and LUCKYCAT scenes). NeRO [Liu et al. 2023] can also produce reasonable results but loses many geometric details, such as the characters in the LUCKYCAT and BRASSGOURD scenes. Our method produces plausible relighting results (shown in the right column of Fig. 9), demonstrating the accuracy of estimated materials.

We also evaluate our method on recent Stanford-ORB [Kuang et al. 2024] dataset. We choose five typical objects with masks. For each object, we randomly select one environment light for training and

the other two lights for relighting. The quantitative measurements of the geometry reconstruction and relighting results are shown in Tab. 3. Our method outperforms NeRO [Liu et al. 2023] on all five scenes. The visual results are shown in Fig 10. NeRO [Liu et al. 2023] produces erroneous surfaces in the TEAPOT and CACTUS scenes, and over-smoothed results in the GNOME scene. Our method can restore decent object geometries and materials, leading to plausible relighting results.

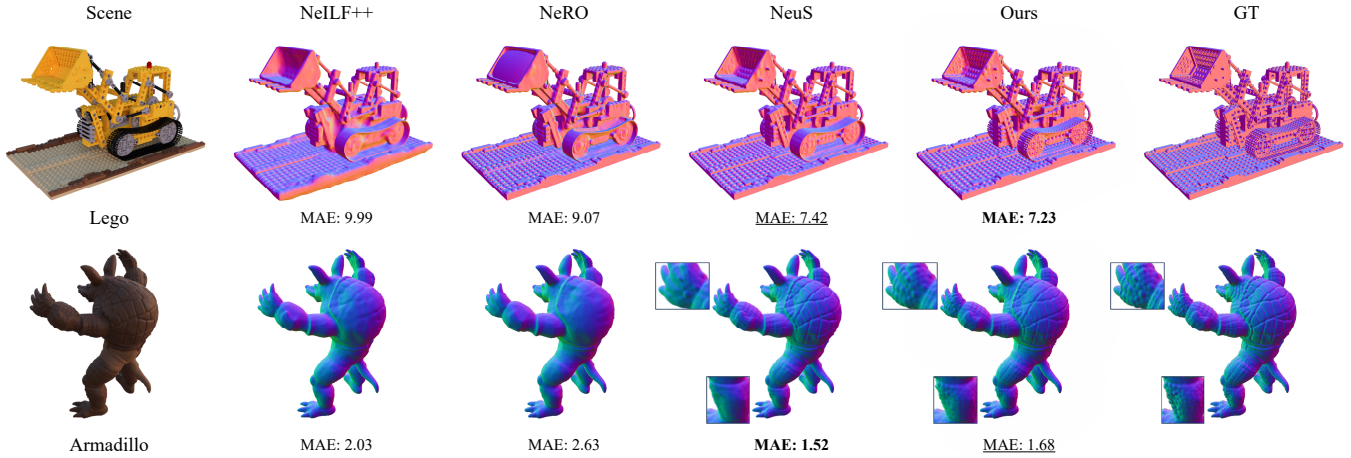


Fig. 6. Comparison of geometry reconstruction among our method, NeILF++ [Zhang et al. 2023], NeRO [Liu et al. 2023] and NeuS [Wang et al. 2021] on scenes from TensorIR [Jin et al. 2023].

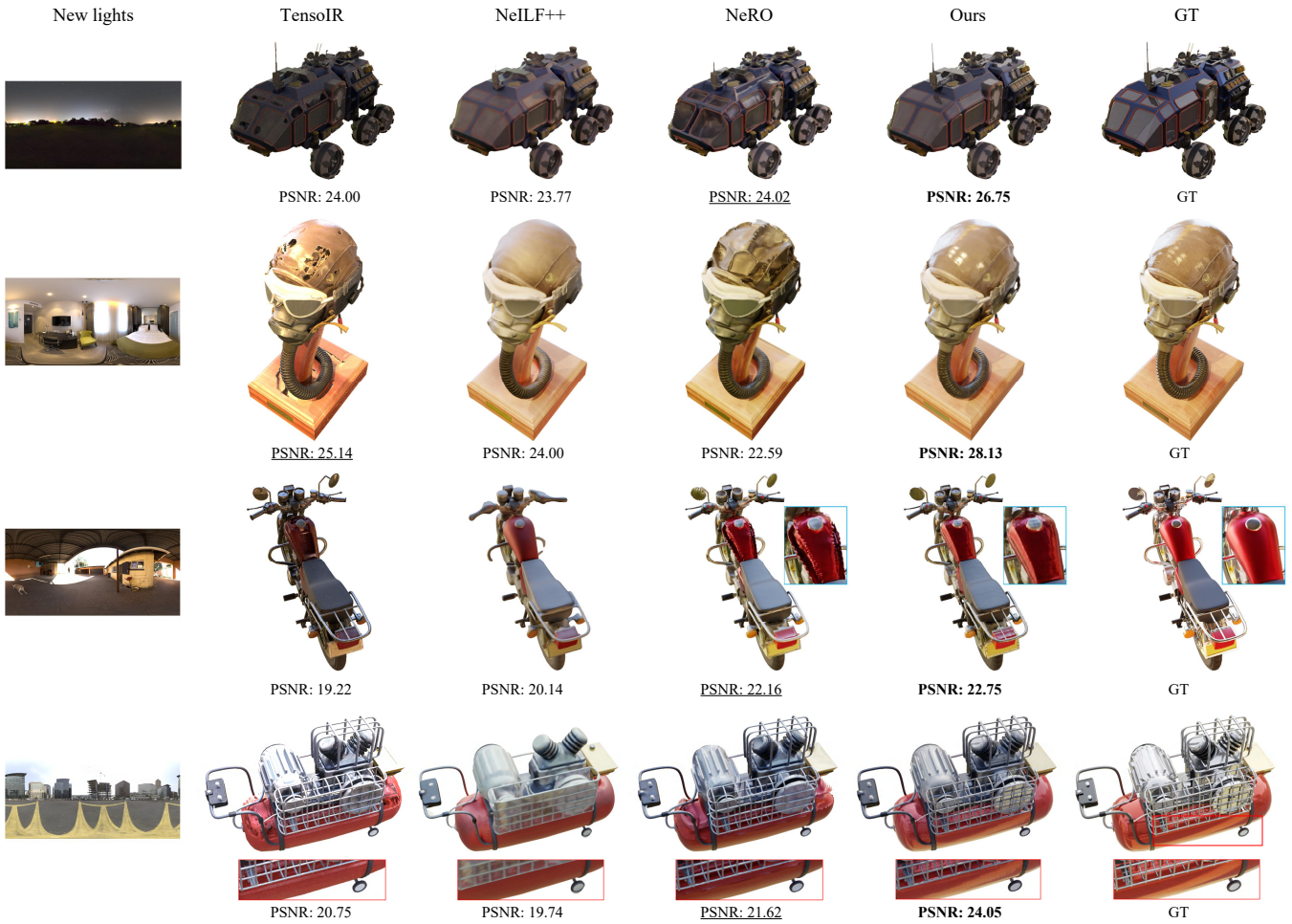


Fig. 7. Comparison of relighting results among our method, TensorIR [Jin et al. 2023], NeILF++ [Zhang et al. 2023] and NeRO [Liu et al. 2023] on our synthetic dataset.

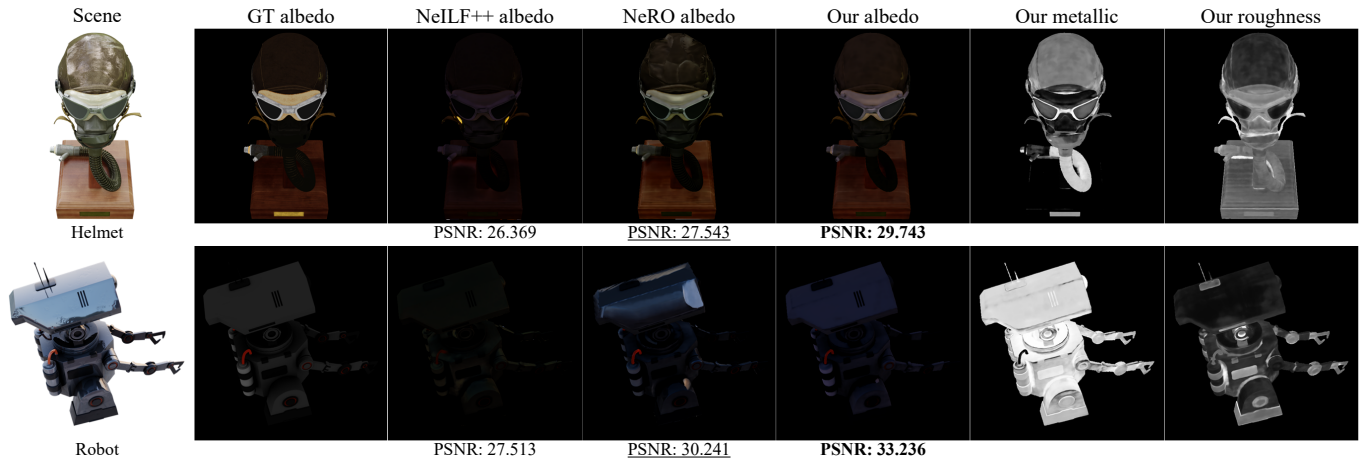


Fig. 8. Comparison of the estimated materials among our method, NeILF++ [Zhang et al. 2023] and NeRO [Liu et al. 2023] on HELMET and ROBOT scenes. The PSNR metric is calculated between the estimated albedo after re-scaling and ground-truth albedo, as done in TensoIR [Jin et al. 2023].

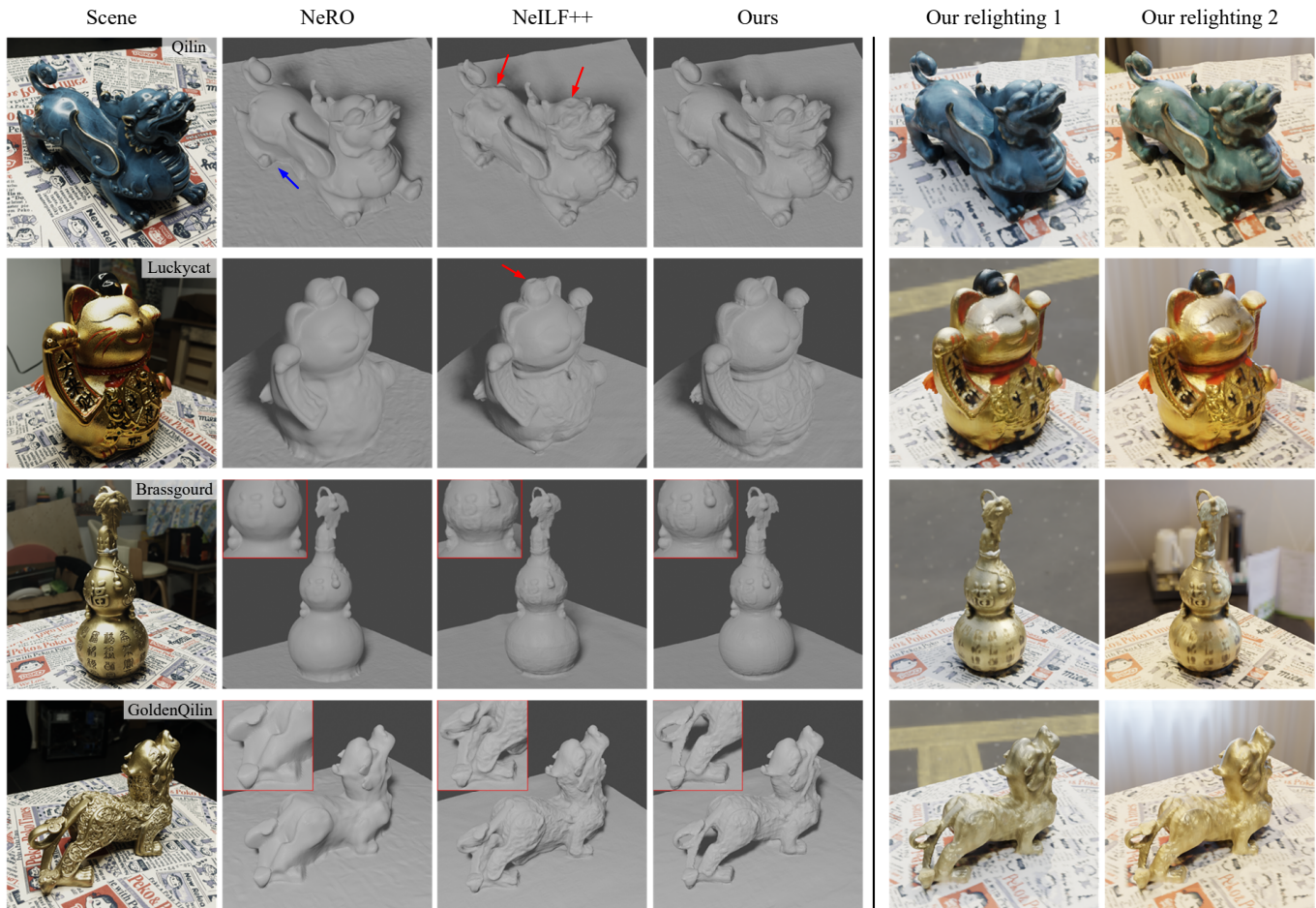


Fig. 9. Visual comparison of geometry reconstruction among our method, NeRO [Liu et al. 2023] and NeILF++ [Zhang et al. 2023] and our relighting results on the real data from NeILF++ [Zhang et al. 2023]. Note that the input images of our method and NeRO [Liu et al. 2023] are LDR images, while NeILF++ [Zhang et al. 2023] uses the HDR images following the official implementation.

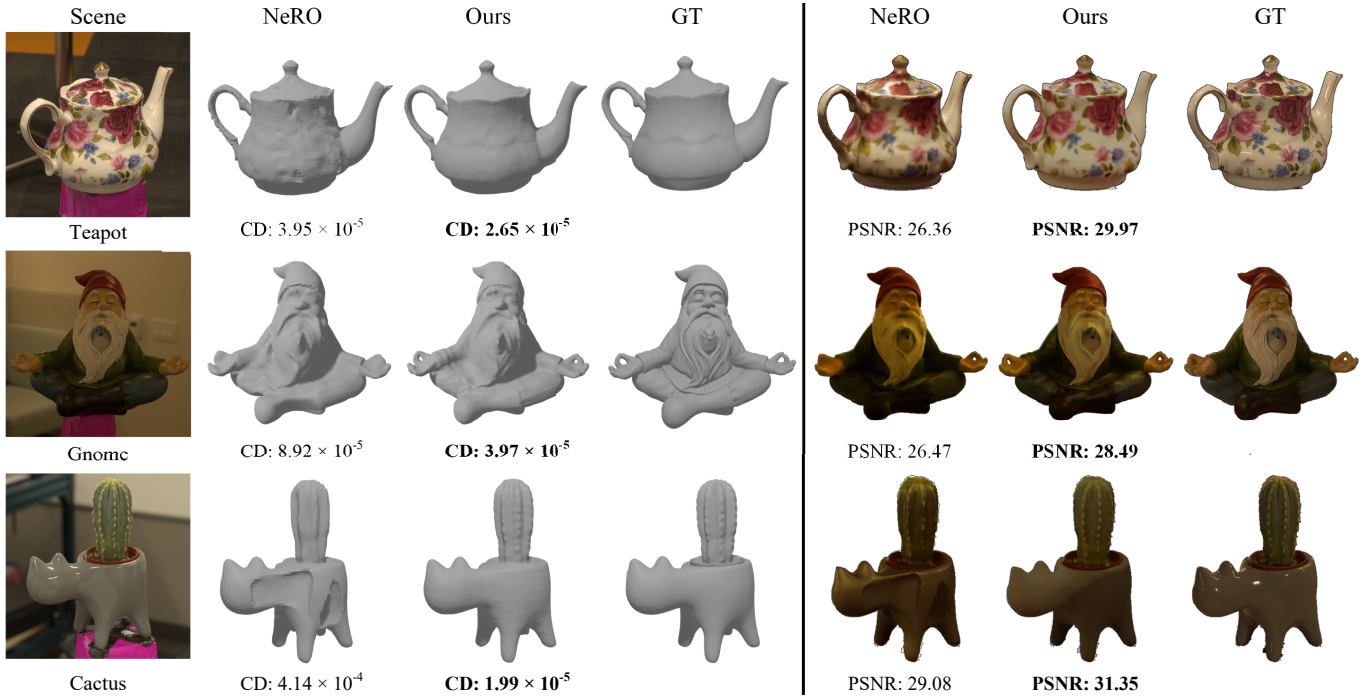


Fig. 10. Comparison of the geometry reconstruction (Left) and relighting results (Right) between our method and NeRO [Liu et al. 2023] on Stanford-ORB [Kuang et al. 2024] dataset. The PSNR metric is averaged on two environment lights.

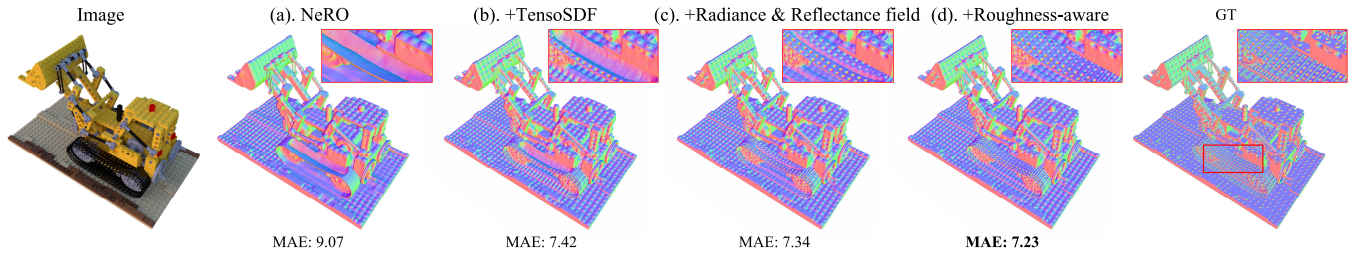


Fig. 11. Ablation studies on the geometry reconstruction. Introducing the TensoSDF (b) can reconstruct more details than NeRO [Liu et al. 2023] (a) but with problematic surfaces. After combining the radiance field and reflectance field with a fixed balancing weight of 0.5 (c), the surface quality can be improved, but still with some flaws. Finally, using the roughness as the weight (d) achieves the best quality.

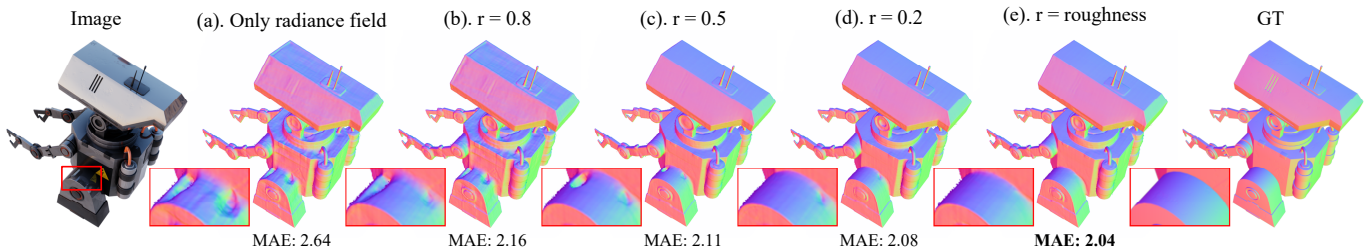


Fig. 12. Ablation studies on the different balancing weights. With the radiance field only (a), i.e., $r = 1$, the reconstructed geometry shows apparent flaws on the reflective surface. With the balancing weights decrease (b-d), the reconstructed quality gradually improves. Using the roughness as the weight (e) achieves the best quality.

Table 3. Geometry reconstruction quality in terms of $CD\downarrow$ ($\times 10^{-4}$) metric and relighting quality in terms of PSNR, SSIM and LPIPS \downarrow metrics on the Stanford-ORB [Kuang et al. 2024] dataset. **Bold** means the best quality.

	$CD\downarrow$		PSNR		SSIM		LPIPS \downarrow	
	NeRO / Ours	NeRO / Ours	NeRO / Ours	NeRO / Ours	NeRO / Ours	NeRO / Ours	NeRO / Ours	NeRO / Ours
Teapot	0.395 / 0.265	26.369 / 29.971	0.978 / 0.986	0.0344 / 0.0276				
Gnome	0.892 / 0.396	26.465 / 28.488	0.929 / 0.956	0.1082 / 0.0947				
Cactus	4.144 / 0.199	29.081 / 31.351	0.977 / 0.984	0.0399 / 0.0362				
Car	0.588 / 0.349	27.763 / 28.010	0.979 / 0.981	0.0350 / 0.0367				
Grogu	4.804 / 3.968	27.081 / 30.595	0.983 / 0.990	0.0396 / 0.0362				
Avg.	2.165 / 1.035	27.352 / 29.683	0.969 / 0.979	0.0514 / 0.0463				

Table 4. The impact of our mesh-SDF fusion strategy for the relighting results on the DRAGON and ROVER scenes. **Bold** means the best quality.

Scene	mesh-SDF fusion	PSNR	SSIM	LPIPS \downarrow
Dragon	\times	27.396	0.935	0.081
	\checkmark	27.899	0.936	0.078
Rover	\times	26.466	0.933	0.060
	\checkmark	26.754	0.935	0.059

6.4 Ablation study

We validate the key components of our method in Fig. 11 step by step. Starting from NeRO [Liu et al. 2023], we replace its pure MLP-based geometry representation with our TensoSDF. The TensoSDF can reconstruct more geometric details and significantly improves the quality (1.65 in MAE). Moreover, TensoSDF reduces the training time to about 50%, from 8 hours to less than 4 hours for each scene in our synthetic dataset. However, the reconstructed geometry still exhibits a noticeable dent on the surface. Then, after introducing both radiance and reflectance fields with a constant weight (0.5 in practice), the surface artifacts are alleviated. Finally, replacing the constant weight with the estimated roughness forms our complete solution and closely matches the ground truth.

To further study the effectiveness of our roughness-aware balancing strategy, we provide ablation studies on different balancing weights, as shown in Fig. 12. We first set the weight $r = 1$, i.e., the radiance field only, showing apparent flaws on the reflective surfaces. With the weights decreasing and approaching the surface roughness, the reconstructed quality becomes better. When setting the balancing weight as the roughness, the quality achieves the best.

Another critical strategy in our material estimation stage is the mesh-SDF fusion. We show its impact on the estimated roughness (Fig. 13) and relighting results (Tab. 4). Without the mesh-SDF fusion, there are many apparent biases, mainly caused by the geometry degradation. The mesh-SDF fusion can reduce these biases, further improving the quality of reconstructed materials and relighting results.

We also present the ablation of our two smoothness priors in Fig. 14. Directly using the explicit representation without any smoothness priors easily causes noise on the reconstructed geometry, especially on flat surfaces. The mipmapping strategy of the tensor grid alleviates this problem during inference, and equipping the Gaussian smooth loss in training can produce smoother results.

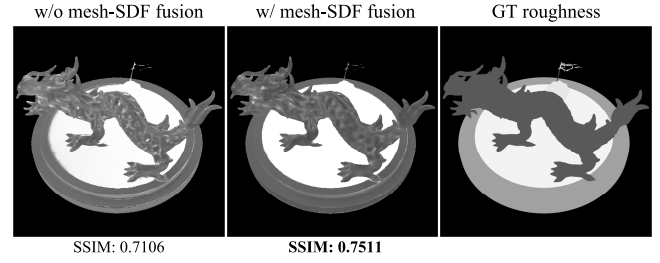


Fig. 13. The impact of our mesh-SDF fusion strategy for estimated roughness. The result without the mesh-SDF fusion (left column) shows obvious bias, while applying the mesh-SDF fusion (middle column) can better match the ground truth (right column).

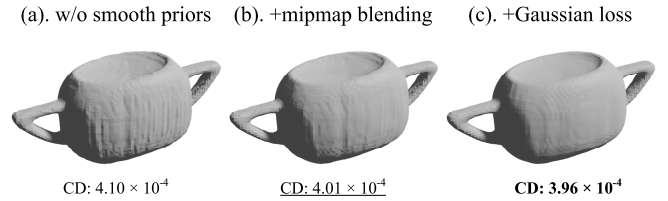


Fig. 14. The impact of our two smoothness priors. Reconstructing object geometry using explicit representation without any smooth priors causes noise on the smooth surface (a), while applying the mipmapping strategy alleviates this problem (b). Finally, introducing the Gaussian smooth loss in training (c) produces the smoothest result.

6.5 Discussion and limitations

Although the high-capacity TensoSDF improves the geometric details and speeds up the training, it still introduces some limitations. One problem is the trade-off between fine details and high-frequency noise. Explicit representations are more prone to over-fitting locally, which inevitably leads to noise. A common mitigation is to use additional smooth regularization, such as our Gaussian smooth loss and mipmapping strategy. However, smooth priors also easily cause the loss of details, as shown in Fig. 15. We leave this problem for future work.

The other problem is the trade-off between the quality and storage. Though the tensorial representation is compact compared to volume-based representations, the storage cost is higher than MLP-based methods. We analyze this trade-off on different resolutions of the tensor grid, as shown in Tab. 5. With the resolution increasing, the reconstructed geometry quality improves while the storage increases. However, even on resolution 200×200 , our method can still produce decent results. One possible solution to reduce storage further is pruning; we leave this for future work.

7 CONCLUSION AND FUTURE WORK

In this paper, we have presented a new framework for robust geometry and material reconstruction. The geometry is represented by a tensorial-encoding SDF field, which obtains more geometric details and reduces the training time. By incorporating the radiance and reflectance fields in a roughness-aware manner, our method is able to reconstruct any reflective objects robustly. Furthermore, we

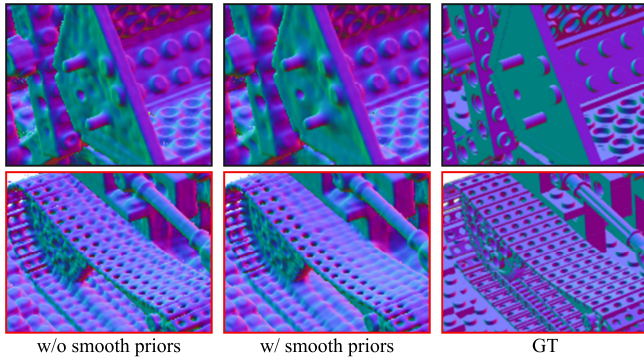


Fig. 15. The trade-offs between the geometric details and noise. The smooth priors can alleviate the noise problem introduced from the explicit representation (first row) while also causing the loss of details (second row).

Table 5. The trade-offs between the geometry quality and storage. *Ours-200* means that the final resolution of the tensor grid is 200×200 . With the resolution increasing, the normal MAE of the reconstructed result decreases, while the model size becomes larger. The results are from the COMPRESSOR scene. **Bold** means the best performance and underline means the second best.

	NeRO	TensoIR	Ours-200	Ours-300	Ours-512
MAE↓	9.18	5.09	3.96	<u>3.64</u>	3.48
Size (MB)↓	8.3	70.5	<u>17.9</u>	37.6	109.0

have designed a mesh-SDF fusion strategy for material estimation, improving the quality of estimated materials. We have demonstrated that our method can achieve more robust geometry reconstruction and outperform the existing state-of-the-art methods in terms of relighting quality.

There are still many potential future researching directions. Regarding the training time, combining our method with the popular 3D Gaussian splatting [Kerbl et al. 2023] may reduce the training time further. For the reconstruction quality, the efficient tensorial representation provides an opportunity to jointly update the geometry and material in the second stage, which may improve the reconstruction quality. From the perspective of diversity, reconstructing translucent objects is also worth researching. However, translucent materials need to consider higher dimensions, and designing an efficient formulation is the key. Our method currently focuses on single-object reconstruction with multi-view inputs. It would be interesting to apply our method on multi-object environments or few-shot reconstruction.

ACKNOWLEDGMENTS

We thank the reviewers for the valuable comments, and XiaoLong Wu for his help in our video. This work has been partially supported by the National Science and Technology Major Project under grant No. 2022ZD0116305 and National Natural Science Foundation of China under grant No. 62272275 and 62172220.

REFERENCES

- Jonathan T Barron and Ben Poole. 2016. The fast bilateral solver. In *European conference on computer vision*. Springer, 617–632.
- Michael Bleyer, Christoph Rhemann, and Carsten Rother. 2011. Patchmatch stereo-stereo matching with slanted support windows. In *Bmvc*, Vol. 11. 1–11.
- Mark Boss, Raphael Braun, Varun Jampani, Jonathan T Barron, Ce Liu, and Hendrik Lensch. 2021a. Nerf: Neural reflectance decomposition from image collections. In *Proceedings of the IEEE/CVF International Conference on Computer Vision*. 12684–12694.
- Mark Boss, Varun Jampani, Raphael Braun, Ce Liu, Jonathan Barron, and Hendrik Lensch. 2021b. Neural-pil: Neural pre-integrated lighting for reflectance decomposition. *Advances in Neural Information Processing Systems* 34 (2021), 10691–10704.
- Neill DF Campbell, George Vogiatzis, Carlos Hernández, and Roberto Cipolla. 2008. Using multiple hypotheses to improve depth-maps for multi-view stereo. In *Computer Vision—ECCV 2008: 10th European Conference on Computer Vision, Marseille, France, October 12–18, 2008, Proceedings, Part I 10*. Springer, 766–779.
- Anpei Chen, Zexiang Xu, Andreas Geiger, Jingyi Yu, and Hao Su. 2022. Tensorf: Tensorial radiance fields. In *European Conference on Computer Vision*. Springer, 333–350.
- Robert L Cook and Kenneth E. Torrance. 1982. A reflectance model for computer graphics. *ACM Transactions on Graphics (ToG)* 1, 1 (1982), 7–24.
- Yasutaka Furukawa and Jean Ponce. 2007. Accurate, Dense, and Robust Multi-View Stereopsis. In *2007 IEEE Conference on Computer Vision and Pattern Recognition*. 1–8. <https://doi.org/10.1109/CVPR.2007.383246>
- David Gallup, Jan-Michael Frahm, Philippos Mordohai, Qingxiong Yang, and Marc Pollefeys. 2007. Real-time plane-sweeping stereo with multiple sweeping directions. In *2007 IEEE Conference on Computer Vision and Pattern Recognition*. IEEE, 1–8.
- Carlo Gatta, Alessandro Rizzi, and Daniele Marini. 2002. ACE: An Automatic Color Equalization Algorithm. In *CGIV*. 316–320.
- Amos Gropp, Lior Yariv, Niv Haim, Matan Atzmon, and Yaron Lipman. 2020. Implicit geometric regularization for learning shapes. *arXiv preprint arXiv:2002.10099* (2020).
- Jon Hasselgren, Nikolai Hofmann, and Jacob Munkberg. 2022. Shape, light, and material decomposition from images using Monte Carlo rendering and denoising. *Advances in Neural Information Processing Systems* 35 (2022), 22856–22869.
- Asmaa Hosni, Christoph Rhemann, Michael Bleyer, Carsten Rother, and Margrit Gelautz. 2012. Fast cost-volume filtering for visual correspondence and beyond. *IEEE transactions on pattern analysis and machine intelligence* 35, 2 (2012), 504–511.
- Haian Jin, Isabella Liu, Peijia Xu, Xiaoshuai Zhang, Songfang Han, Sai Bi, Xiaowei Zhou, Zexiang Xu, and Hao Su. 2023. TensoIR: Tensorial Inverse Rendering. In *Proceedings of the IEEE/CVF Conference on Computer Vision and Pattern Recognition*. 165–174.
- James T Kajiya. 1986. The rendering equation. In *Proceedings of the 13th annual conference on Computer graphics and interactive techniques*. 143–150.
- Brian Karis and Epic Games. 2013. Real shading in unreal engine 4. *Proc. Physically Based Shading Theory Practice* 4, 3 (2013), 1.
- Bernhard Kerbl, Georgios Kopanas, Thomas Leimkühler, and George Drettakis. 2023. 3D Gaussian Splatting for Real-Time Radiance Field Rendering. *ACM Transactions on Graphics* 42, 4 (2023).
- Diederik P Kingma and Jimmy Ba. 2014. Adam: A method for stochastic optimization. *arXiv preprint arXiv:1412.6980* (2014).
- Zhengfei Kuang, Yunzhi Zhang, Hong-Xing Yu, Samir Agarwala, Elliott Wu, Jiajun Wu, et al. 2024. Stanford-ORB: A Real-World 3D Object Inverse Rendering Benchmark. *Advances in Neural Information Processing Systems* 36 (2024).
- Zhaoshuo Li, Thomas Müller, Alex Evans, Russell H Taylor, Mathias Unberath, Ming-Yu Liu, and Chen-Hsuan Lin. 2023. Neuralangelo: High-Fidelity Neural Surface Reconstruction. In *Proceedings of the IEEE/CVF Conference on Computer Vision and Pattern Recognition*. 8456–8465.
- Yuan Liu, Peng Wang, Cheng Lin, Xiaoxiao Long, Jiepeng Wang, Lingjie Liu, Taku Komura, and Wenping Wang. 2023. NeRO: Neural Geometry and BRDF Reconstruction of Reflective Objects from Multiview Images. *arXiv preprint arXiv:2305.17398* (2023).
- William E Lorensen and Harvey E Cline. 1998. Marching cubes: A high resolution 3D surface construction algorithm. In *Seminal graphics: pioneering efforts that shaped the field*. 347–353.
- Ben Mildenhall, Pratul P Srinivasan, Matthew Tancik, Jonathan T Barron, Ravi Ramamoorthi, and Ren Ng. 2021. Nerf: Representing scenes as neural radiance fields for view synthesis. *Commun. ACM* 65, 1 (2021), 99–106.
- Thomas Müller, Alex Evans, Christoph Schied, and Alexander Keller. 2022. Instant neural graphics primitives with a multiresolution hash encoding. *ACM Transactions on Graphics (ToG)* 41, 4 (2022), 1–15.
- Michael Niemeyer, Lars Mescheder, Michael Oechsle, and Andreas Geiger. 2020. Differentiable volumetric rendering: Learning implicit 3d representations without 3d supervision. In *Proceedings of the IEEE/CVF Conference on Computer Vision and Pattern Recognition*. 3504–3515.
- Michael Oechsle, Songyou Peng, and Andreas Geiger. 2021. Unisurf: Unifying neural implicit surfaces and radiance fields for multi-view reconstruction. In *Proceedings of*

- the *IEEE/CVF International Conference on Computer Vision*. 5589–5599.
- Adam Paszke, Sam Gross, Francisco Massa, Adam Lerer, James Bradbury, Gregory Chanan, Trevor Killeen, Zeming Lin, Natalia Gimelshein, Luca Antiga, et al. 2019. Pytorch: An imperative style, high-performance deep learning library. *Advances in neural information processing systems* 32 (2019).
- Christian Richardt, Douglas Orr, Ian Davies, Antonio Criminisi, and Neil A Dodgson. 2010. Real-time spatiotemporal stereo matching using the dual-cross-bilateral grid. In *Computer Vision—ECCV 2010: 11th European Conference on Computer Vision, Heraklion, Crete, Greece, September 5–11, 2010, Proceedings, Part III 11*. Springer, 510–523.
- Johannes L Schonberger and Jan-Michael Frahm. 2016. Structure-from-motion revisited. In *Proceedings of the IEEE conference on computer vision and pattern recognition*. 4104–4113.
- Pratul P Srinivasan, Boyang Deng, Xiuming Zhang, Matthew Tancik, Ben Mildenhall, and Jonathan T Barron. 2021. Nerv: Neural reflectance and visibility fields for relighting and view synthesis. In *Proceedings of the IEEE/CVF Conference on Computer Vision and Pattern Recognition*. 7495–7504.
- Christoph Strecha, Rik Fransens, and Luc Van Gool. 2006. Combined depth and outlier estimation in multi-view stereo. In *2006 IEEE Computer Society Conference on Computer Vision and Pattern Recognition (CVPR'06)*, Vol. 2. IEEE, 2394–2401.
- Cheng Sun, Min Sun, and Hwann-Tzong Chen. 2022. Direct voxel grid optimization: Super-fast convergence for radiance fields reconstruction. In *Proceedings of the IEEE/CVF Conference on Computer Vision and Pattern Recognition*. 5459–5469.
- Dor Verbin, Peter Hedman, Ben Mildenhall, Todd Zickler, Jonathan T Barron, and Pratul P Srinivasan. 2022. Ref-nerf: Structured view-dependent appearance for neural radiance fields. In *2022 IEEE/CVF Conference on Computer Vision and Pattern Recognition (CVPR)*. IEEE, 5481–5490.
- Peng Wang, Lingjie Liu, Yuan Liu, Christian Theobalt, Taku Komura, and Wenping Wang. 2021. Neus: Learning neural implicit surfaces by volume rendering for multi-view reconstruction. *arXiv preprint arXiv:2106.10689* (2021).
- Yiming Wang, Qin Han, Marc Habermann, Kostas Daniilidis, Christian Theobalt, and Lingjie Liu. 2023. Neus2: Fast learning of neural implicit surfaces for multi-view reconstruction. In *Proceedings of the IEEE/CVF International Conference on Computer Vision*. 3295–3306.
- Zhou Wang, Alan C Bovik, Hamid R Sheikh, and Eero P Simoncelli. 2004. Image quality assessment: from error visibility to structural similarity. *IEEE transactions on image processing* 13, 4 (2004), 600–612.
- Tong Wu, Jiaqi Wang, Xingang Pan, Xudong Xu, Christian Theobalt, Ziwei Liu, and Dahua Lin. 2022. Voxurf: Voxel-based efficient and accurate neural surface reconstruction. *arXiv preprint arXiv:2208.12697* (2022).
- Yao Yao, Jingyang Zhang, Jingbo Liu, Yihang Qu, Tian Fang, David McKinnon, Yanghai Tsin, and Long Quan. 2022. NeIf: Neural incident light field for physically-based material estimation. In *European Conference on Computer Vision*. Springer, 700–716.
- Lior Yariv, Jiatao Gu, Yoni Kasten, and Yaron Lipman. 2021. Volume rendering of neural implicit surfaces. *Advances in Neural Information Processing Systems* 34 (2021), 4805–4815.
- Lior Yariv, Peter Hedman, Christian Reiser, Dor Verbin, Pratul P Srinivasan, Richard Szeliski, Jonathan T Barron, and Ben Mildenhall. 2023. BakedSDF: Meshing Neural SDFs for Real-Time View Synthesis. *arXiv preprint arXiv:2302.14859* (2023).
- Lior Yariv, Yoni Kasten, Dror Moran, Meirav Galun, Matan Atzmon, Basri Ronen, and Yaron Lipman. 2020. Multiview neural surface reconstruction by disentangling geometry and appearance. *Advances in Neural Information Processing Systems* 33 (2020), 2492–2502.
- Jingyang Zhang, Yao Yao, Shiwei Li, Tian Fang, David McKinnon, Yanghai Tsin, and Long Quan. 2022b. Critical regularizations for neural surface reconstruction in the wild. In *Proceedings of the IEEE/CVF Conference on Computer Vision and Pattern Recognition*. 6270–6279.
- Jingyang Zhang, Yao Yao, Shiwei Li, Jingbo Liu, Tian Fang, David McKinnon, Yanghai Tsin, and Long Quan. 2023. NeLLF++: Inter-Reflectable Light Fields for Geometry and Material Estimation. *arXiv preprint arXiv:2303.17147* (2023).
- Kai Zhang, Fujun Luan, Qianqian Wang, Kavita Bala, and Noah Snavely. 2021a. PhysG: Inverse rendering with spherical gaussians for physics-based material editing and relighting. In *Proceedings of the IEEE/CVF Conference on Computer Vision and Pattern Recognition*. 5453–5462.
- Richard Zhang, Phillip Isola, Alexei A Efros, Eli Shechtman, and Oliver Wang. 2018. The unreasonable effectiveness of deep features as a perceptual metric. In *Proceedings of the IEEE conference on computer vision and pattern recognition*. 586–595.
- Xiuming Zhang, Pratul P Srinivasan, Boyang Deng, Paul Debevec, William T Freeman, and Jonathan T Barron. 2021b. Nerfactor: Neural factorization of shape and reflectance under an unknown illumination. *ACM Transactions on Graphics (ToG)* 40, 6 (2021), 1–18.
- Yuanqing Zhang, Jiaming Sun, Xingyi He, Huan Fu, Rongfei Jia, and Xiaowei Zhou. 2022a. Modeling indirect illumination for inverse rendering. In *Proceedings of the IEEE/CVF Conference on Computer Vision and Pattern Recognition*. 18643–18652.

Supplementary Material – TensoSDF: Roughness-aware Tensorial Representation for Robust Geometry and Material Reconstruction

JIA LI, School of Software, Shandong University, China

LU WANG[†], School of Software, Shandong University, China

LEI ZHANG, The Hong Kong Polytechnic University, China

BEIBEI WANG[†], School of Intelligence Science and Technology, Nanjing University, China

1 RESULTS

1.1 Reconstructed geometry evaluation

We provide additional comparisons of the reconstructed geometry results on our synthetic dataset in Fig. 2. From the results, our method can not only reconstruct the surfaces with strong reflection in all scenes but also recover richer geometric details (COMPRESSOR, HELMET and DRAGON scenes, etc.). On the MOTOR and DRAGON scenes, our results are slightly higher than NeuS [Wang et al. 2021] in MAE metric, mainly due to the noise problem, although our results are more detailed and closer to the ground truth visually.

1.2 Estimated material evaluation

We evaluate relighting quality on our synthetic dataset in terms of LPIPS [Zhang et al. 2018] in Tab. 1. Our method outperforms all the baseline methods. The visual results are shown in Fig. 3. By comparison, our method can produce decent reflection and highlights (such as COMPRESSOR, HELMET and ROVER scenes, etc.) based on the estimated materials, while the other methods either suffer from erroneous surfaces or tend to produce blurred reflections.

1.3 Results on real data

We provide additional qualitative geometry and relighting results on the real data from NeILF++ [Zhang et al. 2023] in Fig. 4. All results are reconstructed from LDR images. Our method is able to produce realistic relighting results based on our robust geometry and material reconstruction.

1.4 Ablation studies on the shared tensor grid

We adopt a shared tensor grid to encode geometry and appearance jointly in our TensoSDF representation, which can enhance the correlation between the geometry and appearance, while TensoRF [Chen et al. 2022] uses two tensor grids to encode separately. We compare these two choices in Fig. 1. From the results, using one shared tensor grid can improve the quality of reconstructed geometry.

REFERENCES

Anpei Chen, Zexiang Xu, Andreas Geiger, Jingyi Yu, and Hao Su. 2022. TensorRF: Tensorial radiance fields. In *European Conference on Computer Vision*. Springer, 333–350.

[†]Corresponding authors.

Authors' addresses: Jia Li, School of Software, Shandong University, China, riga27527@gmail.com; Lu Wang[†], School of Software, Shandong University, China, luwang_hcivr@sdu.edu.cn; Lei Zhang, The Hong Kong Polytechnic University, China, cslzhang@comp.polyu.edu.hk; Beibei Wang[†], School of Intelligence Science and Technology, Nanjing University, China, beibei.wang@nju.edu.cn.

Table 1. Relighting quality in terms of LPIPS↓ on our synthetic dataset. **Bold** means the best performance and underline means the second best.

	TensoIR	NeRO	NeILF++	Ours
Rover	0.0801	<u>0.0693</u>	0.0754	0.0593
Dragon	0.1302	<u>0.0898</u>	0.0988	0.0775
Motor	0.0821	<u>0.0702</u>	0.0870	0.0681
Helmet	<u>0.1040</u>	0.1079	0.1056	0.0770
Robot	0.0931	<u>0.0755</u>	0.0782	0.0613
Compressor	<u>0.1038</u>	0.1073	0.1286	0.0830
Avg.	0.0989	<u>0.0867</u>	0.0956	0.0710

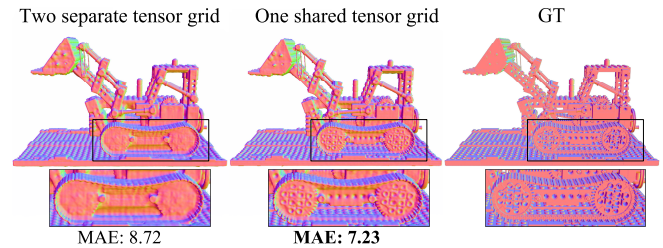


Fig. 1. The impact of the shared tensor grid. Compared to directly using two separate tensor grids to encode geometry and appearance respectively (left column), using one shared tensor grid can improve the quality of geometry reconstruction (right column).

Haian Jin, Isabella Liu, Peijia Xu, Xiaoshuai Zhang, Songfang Han, Sai Bi, Xiaowei Zhou, Zexiang Xu, and Hao Su. 2023. TensoIR: Tensorial Inverse Rendering. In *Proceedings of the IEEE/CVF Conference on Computer Vision and Pattern Recognition*. 165–174.

Yuan Liu, Peng Wang, Cheng Lin, Xiaoxiao Long, Jiepeng Wang, Lingjie Liu, Taku Komura, and Wenping Wang. 2023. NeRO: Neural Geometry and BRDF Reconstruction of Reflective Objects from Multiview Images. *arXiv preprint arXiv:2305.17398* (2023).

Peng Wang, Lingjie Liu, Yuan Liu, Christian Theobalt, Taku Komura, and Wenping Wang. 2021. Neus: Learning neural implicit surfaces by volume rendering for multi-view reconstruction. *arXiv preprint arXiv:2106.10689* (2021).

Jingyang Zhang, Yao Yao, Shiwei Li, Jingbo Liu, Tian Fang, David McKinnon, Yanghai Tsin, and Long Quan. 2023. NeILF++: Inter-Reflectable Light Fields for Geometry and Material Estimation. *arXiv preprint arXiv:2303.17147* (2023).

Richard Zhang, Phillip Isola, Alexei A Efros, Eli Shechtman, and Oliver Wang. 2018. The unreasonable effectiveness of deep features as a perceptual metric. In *Proceedings of the IEEE conference on computer vision and pattern recognition*. 586–595.



Fig. 2. Comparison of geometry reconstruction among our method, TensoIR [Jin et al. 2023], NeRO [Liu et al. 2023], NeLF++ [Zhang et al. 2023] and NeuS [Wang et al. 2021] on our synthetic dataset.



Fig. 3. Comparison of relighting results among our method, TensoIR [Jin et al. 2023], NeLF++ [Zhang et al. 2023] and NeRO [Liu et al. 2023] on our synthetic dataset.

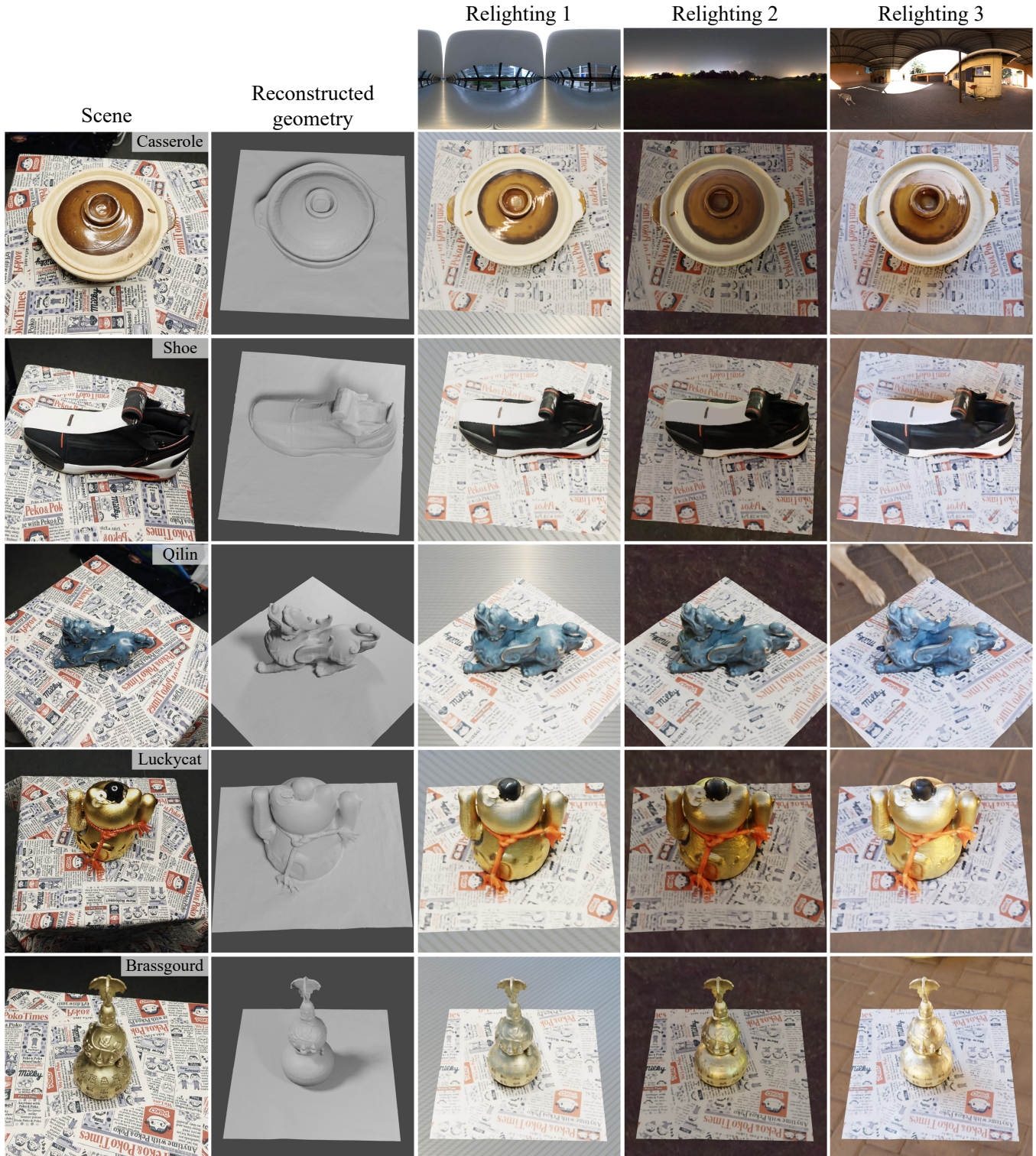


Fig. 4. Our reconstructed geometry and relighting results on the real data from NeLF++ [Zhang et al. 2023]. All results are reconstructed from LDR images.